Article:
Symonds, CC orcid.org/0000-0001-7952-3805, Makhov, DV, Cole-Filipiak, NC et al. (3 more authors) (2019) Ultrafast photodissociation dynamics of pyrazole, imidazole and their deuterated derivatives using ab initio multiple cloning. Physical chemistry chemical physics : PCCP, 21 (19). pp. 9987-9995. ISSN 1463-9076

https://doi.org/10.1039/c9cp00039a

Ultrafast Photodissociation Dynamics of Pyrazole, Imidazole and their Deuterated Derivatives using *Ab Initio* Multiple Cloning-

Electronic Supplemental Information

Christopher C. Symonds,* Dmitry V. Makhov,, Neil C. Cole-Filipiak, James A. Green,
Vasilios G. Stavros, and Dmitrii V. Shalashilin.*

ESI-1 Numerical Details

ESI-1.1 Working Equations

Full derivation of the the AIMC method has been presented elsewhere [1,2], and as such the working equations will be presented here without proof. The AIMC method, like the MCE method before it [3,4], uses a linear combination of Ehrenfest configurations $|\psi_k\rangle$ as the ansatz for the wavefunction coupled to time-dependent amplitudes D_k and summed over K configurations

$$\begin{aligned} |\Psi\rangle &= \sum_{k=1}^{K} D_k(t)\,|\psi_k\rangle \\ &= \sum_{k=1}^{K} D_k(t)\left[\sum_{r=1}^{R} a_{rk}(t)\,|\phi_r\rangle\right]|\mathbf{z}_k\rangle\,. \end{aligned} \tag{1}$$

The Ehrenfest configuration splits the wavefunction into nuclear and electronic parts with $|\phi_r\rangle$ being the rth of a superposition of R orthonormal electronic states coupled to time-dependent amplitudes $a_{rk}(t)$, and with the nuclear part being supplied by the trajectory guided gaussian basis $|\mathbf{z}_k(t)\rangle$ centred in phase space at coordinates and momenta $(\mathbf{q}_k,\mathbf{p}_k)$ such that, in coordinate representation,

$$\langle\mathbf{q}|\mathbf{z}_k(\mathbf{q}_k,\mathbf{p}_k)\rangle = \left(\frac{\gamma}{\pi}\right)^{N/4}\exp\left(\frac{\gamma}{2}(\mathbf{q}-\mathbf{q}_k)^2+\frac{i}{\hbar}\mathbf{p}_k(\mathbf{q}-\mathbf{q}_k)+\frac{i}{\hbar}\alpha_k\right). \tag{2}$$

The gaussian basis vectors are multidimensional and can be found as the product of N one-dimensional gaussian basis functions $|\mathbf{z}_k(t)\rangle = \prod_{n=1}^{N}|z_k^{(m)}\rangle$, the width parameter γ can be chosen dependent on the atom [5], and the phase α_k evolves as

$$\frac{\mathrm{d}\alpha_k}{\mathrm{d}t} = \frac{\dot{\mathbf{q}}_k\mathbf{p}_k}{2}. \tag{3}$$

The centers of the gaussian basis $(\mathbf{q}_k,\mathbf{p}_k)$ are guided by Ehrenfest trajectories resembling Newton's equations of motion but with corrections to account for quantum and non-adiabatic effects

$$\dot{\mathbf{q}}_k = \mathbf{p}_k\mathbf{M}^{-1} \tag{4a}$$

$$\dot{\mathbf{p}}_k = \mathbf{F}_k, \tag{4b}$$

where $\mathbf{M}$ is the diagonal matrix of atomic masses and the Ehrenfest force $\mathbf{F}_k$ includes not only the usual gradient term ∇_q and adiabatic electronic energy $V_r(\mathbf{q}_k)$, but also a second term related to non-adiabatic coupling such that

$$\begin{aligned} \mathbf{F}_k = &\sum_{r=1}^{R} a_{rk}^{*}a_{rk}\nabla_q V_r(\mathbf{q}_k) \\ &+\sum_{r=1}^{R}\sum_{s\neq r}^{R} a_{rk}^{*}a_{sk}\mathbf{d}_{rs}(\mathbf{q}_k)\left[V_r(\mathbf{q}_k)-V_s(\mathbf{q}_k)\right], \end{aligned} \tag{5}$$

where $\mathbf{d}$ is the non-adiabatic coupling vector given by

* Corresponding Authors: C.C.Symonds@leeds.ac.uk, D.Shalashilin@leeds.ac.uk

$$\mathbf{d}_{rs}(\mathbf{q}_k) = \langle \phi_r | \nabla_q | \phi_s \rangle . \tag{6}$$

The evolution of the amplitudes for the electronic states a_{rk} is given by

$$\dot{a}_{rk} = -\frac{i}{\hbar} \sum_{s=1}^{R} H_{rs}^{\mathrm{el}}(\mathbf{z}_k) a_{sk}, \tag{7}$$

where the electronic Hamiltonian has values

$$H_{rs}^{\mathrm{el}}(\mathbf{z}_k) = \begin{cases} V_r(\mathbf{q}_k) & r = s \\ -i\hbar \mathbf{p}_k \mathbf{d}_{rs}(\mathbf{q}_k) \mathbf{M}^{-1} & r \neq s. \end{cases} \tag{8}$$

The time evolution of the amplitudes a_{rk} reflect the coupling between the electronic states while the coupling between the individual Ehrenfest configurations is provided by the amplitude D_k, which evolves as

$$\sum_{j=1}^{K} \langle \psi_j | \psi_k \rangle \dot{D}_j = -\frac{i}{\hbar} \sum_{k=1}^{K} \left[\langle \psi_j | \hat{H} | \psi_k \rangle - i\hbar \langle \psi_j | \dot{\psi}_k \rangle \right] D_k. \tag{9}$$

The matrix element of the Hamiltonian in the above expression can be expanded as

$$\begin{aligned} \langle \psi_j | \hat{H} | \psi_k \rangle &= \sum_{r,s=1}^{R} a_{rj}^* a_{sk} \langle \mathbf{z}_j \phi_r | \hat{H} | \phi_s \mathbf{z}_k \rangle \\ &= \sum_{r,s=1}^{R} a_{rj}^* a_{sk} \left[\delta_{rs} \langle \mathbf{z}_j | \hat{T} | \mathbf{z}_k \rangle + \delta_{rs} \langle \mathbf{z}_j | V_r(\mathbf{q}) | \mathbf{z}_k \rangle - \hbar^2 \langle \mathbf{z}_j | \mathbf{d}_{rs}(\mathbf{q}) \dot{\mathbf{q}} | \mathbf{z}_k \rangle \right]. \end{aligned} \tag{10}$$

The kinetic energy term can be found analytically as

$$\langle \mathbf{z}_j | \hat{T} | \mathbf{z}_k \rangle = \langle \mathbf{z}_j | \mathbf{z}_k \rangle \frac{\hbar^2 \gamma}{4} (\mathbf{z}_j^* \mathbf{z}_j^* + \mathbf{z}_k \mathbf{z}_k - 2\mathbf{z}_j^* \mathbf{z}_k), \tag{11}$$

where $\mathbf{z}$ is the eigenvalue of the coherent state $|\mathbf{z}\rangle$ given by

$$\mathbf{z} = \sqrt{\frac{\gamma}{2}} \mathbf{q} + \frac{i}{\hbar} \frac{1}{\sqrt{2\gamma}} \mathbf{p}, \tag{12}$$

however the potential energy term and the non-adiabatic coupling matrix element (NACME) must be approximated using a bra-ket averaged Taylor (BAT) expansion [1] which takes the average of two Taylor expansions centred around the maximum of one of the basis functions involved in the matrix element. A first order BAT expansion gives the expression for the potential energy

$$\begin{aligned} \langle \mathbf{z}_j | V_r(\mathbf{q}) | \mathbf{z}_k \rangle \approx \langle \mathbf{z}_j | \mathbf{z}_k \rangle & \left(\frac{V_r(\mathbf{q}_j) + V_r(\mathbf{q}_k)}{2} \right) \\ & + \left(\frac{\langle \mathbf{z}_j | (\mathbf{q} - \mathbf{q}_j) | \mathbf{z}_k \rangle \nabla_q V_r(\mathbf{q}_j) + \langle \mathbf{z}_j | (\mathbf{q} - \mathbf{q}_k) | \mathbf{z}_k \rangle \nabla_q V_r(\mathbf{q}_k)}{2} \right), \end{aligned} \tag{13}$$

while a zeroth order BAT expansion approximates the expression for the NACME as

$$\langle \mathbf{z}_j | \mathbf{d}_{rs}(\mathbf{q}) \dot{\mathbf{q}} | \mathbf{z}_k \rangle \approx \frac{i}{2\hbar} \langle \mathbf{z}_j | \mathbf{z}_k \rangle \left(\dot{\mathbf{q}}_j \mathbf{d}_{rs}(\mathbf{q}_l) + \dot{\mathbf{q}}_k \mathbf{d}_{rs}(\mathbf{q}_k) \right). \tag{14}$$

As the coupling between the Ehrenfest configurations is contained solely within the propagation of the $D_k(t)$ amplitude, this means that each of the Ehrenfest configurations may be propagated individually and then combined once completed through the time dependent $D_k(t)$ amplitudes. As the quantities used in equations 13 and 14 are calculated also in equations 4 - 6 this means that the Ehrenfest configurations can be combined without extra electronic structure calculations provided such data is saved during propagation, greatly reducing the computational expense of combining the Ehrenfest configurations.

ESI-1.2 Cloning Procedure

In all methods based on Ehrenfest dynamics, the wavefunction is propagated not along the potential energy surface classically but on a quantum average of the potential. While this method of propagation has had success in many applications it encounters problems when the Ehrenfest trajectories that guide the wavefunction leave a region of nonadiabatic coupling with significant populations on several electronic states, which are associated with significantly different forces. In this case, the average potential energy surface is not a faithful representation of the system, and so the wavefunction is propagated subject to a force that is an average of different forces on each electronic state and that therefore often does not describe the true dynamics of the wavefunction. To counter this effect, the cloning procedure was developed.

Cloning is a recent inclusion to the MCE method, having been introduced in a coupled coherent states context in 2014 by Makhov *et al.*[1] and first used in the simulation of pyrrole in a paper published the following year.[2]. Cloning takes its inspiration from the Multiple Spawning method of Martínez and Ben-Nun[6–8], and may be viewed simply as a straightforward and convenient way of performing spawning. In the cloning procedure when a basis function leaves an area of non-adiabatic coupling, such as is described above, that basis function is cloned, with one instance projected onto a single potential energy surface, and the other projected onto a linear combination of the remaining potential energy surfaces.

If, before a cloning event, a single basis function is given by

$$|\psi_k(t)\rangle = \left(\sum_{r=1}^{R} a_{rk}\,|\varphi_r\rangle\right)|\mathbf{z}_k(t)\rangle\,, \tag{15}$$

then after cloning two basis functions will exist, given by

$$|\psi'_k\rangle = \left(\frac{a_{rk}}{|a_{rk}|}\,|\phi_r\rangle + \sum_{s\neq r}^{R} 0\times|\phi_s\rangle\right)|\mathbf{z}_k\rangle \tag{16a}$$

$$|\psi''_k\rangle = \left(0\times|\phi_r\rangle + \frac{1}{\sqrt{1-|a_{rk}|^2}}\sum_{s\neq r}^{R} a_{sk}\,|\phi_s\rangle\right)|\mathbf{z}_k\rangle\,. \tag{16b}$$

The multiconfigurational amplitudes are then adjusted to preserve the integrity of the wavefunction such that

$$D'_k = D_k|a_{rk}| \tag{17a}$$

$$D''_k = D_k\sqrt{1-|a_{rk}|^2}. \tag{17b}$$

The determination of when to clone a basis set is dependent upon two quantities, the breaking force $\mathbf{F}^{\mathrm{br}}_{rk}$ and the non-adiabatic coupling $\mathbf{d}_{rs}(\mathbf{q})$. The breaking force for the rth potential energy surface is given as dependent on the difference between the force on the rth potential energy surface and the Ehrenfest average force, such that

$$\begin{aligned}\mathbf{F}^{\mathrm{br}}_{rk} &= a^*_{rk}a_{rk}\Delta\mathbf{F}_{rk}\\ &= a^*_{rk}a_{rk}\left(\nabla_q V_r(\mathbf{q}) - \sum_{s=1}^{R} a^*_{sk}a_{sk}\nabla_q V_s(\mathbf{q}).\right)\end{aligned} \tag{18}$$

Cloning is triggered when the breaking force becomes larger than a critical value and the non-adiabatic coupling is small, such that

$$\begin{aligned}\left|\mathbf{F}^{\mathrm{br}}_{rk}\mathbf{M}^{-1}\right| &> \xi_{cln}\\ |\mathbf{d}_{rs}(\mathbf{q}_k)| &< \xi_{nac}\end{aligned} \tag{19}$$

where the critical values ξ_{cln} and ξ_{nac} are determined empirically. For the simulations carried out on imidazole, pyrazole and their selectively deuterated derivatives the thresholds for cloning were set to $\xi_{\mathrm{clon}} = 5\times10^{-6}$ a.u. and $\xi_{\mathrm{nac}} = 2\times10^{-3}$ a.u. The number of cloning events per branch was restricted to three, to limit the rate of basis set expansion.

The combination of the cloning procedure and the MCE approach has made the AIMC method an extremely powerful technique able to simulate the ultrafast dynamics of small molecules[2,9–11], and it has been demonstrated that for model systems the addition of cloning enables MCE simulations to converge to numerically exact results in systems with tens of degrees of freedom.[12]

ESI-2 Discussion of the Initial State for Dynamics

As detailed in the main article, the simulations were carried out using the S_1 state as a starting state for the trajectories. Excitation by a pump pulse would however be likely to partially populate other electronic states as well, and so a small set of simulations were carried out to investigate the early stage dynamics of the wavefunction when it is placed initially on the S_2 electronic state, simulating the dynamics for 100 trajectories. The population transfer in the first 50 fs for molecules starting on both the S_1 and S_2 states is shown in figure ESI.1a for imidazole and pyrazole, and in figure ESI.1b for the selectively deuterated species of these molecules.

It can be immediately seen that a rapid decay from the S_2 state occurs within the first 10 fs for all molecules when started on the S_2 state which is much smaller than the resolution for the experimental results. Recent work by Green *et al.* has shown that a similar rapid decay is seen in AIMC simulations of 2-ethylpyrrole[11], with the effect of a slight broadening of the TKER spectrum and a minor increase in the H atom appearance lifetime and it is expected that similar behaviour would be seen for both imidazole and pyrazole. It is known that the CASSCF calculations used for the potential energy surfaces introduce some inaccuracies (for example the increase in the peak energy of the TKER spectra in comparison to experiment), and the simple model of initial excitation introduces another minor source of inaccuracy however this source of inaccuracy can be mitigated through the use of the recent Floquet hamiltonian technique presented by Makhov and Shalashilin which more properly simulates an initial excitation laser pulse.[13]

ESI-3 Fits used to find the appearance lifetimes

Figures ESI.2 and ESI.3 show the fits used to find the H/D atom appearance lifetimes from the experimental data and the smoothed transient calculated from the raw AIMC data (as shown in figures 3 and 4 in the main text). In addition to these fits, Figure 2B shows the fit to the experimental data decomposed into the forward and reverse dynamics, the former of which is used to find the appearance lifetime of the D^+ atoms. The fits are found using the kinetic model given as equation 1 in the main text and explained therein. Due to the presence of a background signal associated with reverse dynamics in the imidazole-d_1 experimental data, a modified kinetic model is used, given by equation 2 in the main text.

ESI-4 Consideration of the active space used for the simulation of pyrazole

The active space used for the simulation of pyrazole was the same as that used for imidazole, namely 10 electrons in 8 orbitals, with a basis set based on the cc-pVDZ basis of Dunning but with the addition of extra diffuse functions on the N and H atoms involved in the dissociation mechanism considered in this article, taken from the aug-cc-pVDZ basis set. A notable effect of this choice of basis set and active space was that when the orbitals were calculated, a pair of σ and σ^* orbitals were placed on the N-H bond but not on the N-N bond. In this way, the active space used in the AIMC calculations differs from that used by Xie *et al.*[14] whose MS-CASPT2(10,8) electronic structure calculations placed σ and σ^* orbitals on the N-N bond but not on the N-H bond. This difference in active spaces naturally leads to different results as the simulations are set up to examine different mechanisms (as discussed at length in the main text), however the question of how the choice of the active space influences the results presented in the main text does bear consideration. As such, a set of potential energy cuts were calculated using CASSCF with four different active spaces, which are given in figure ESI.4 along the N-H stretch. For all potential energy cuts the N-H extension is calculated by only moving the H atom and leaving the rest of the molecule stationary. The first potential energy cut, shown in panel A, is the active space and basis set used in the simulations detailed in the main text. This basis set is a combination of the aug-cc-pVDZ basis for the N and H atoms involved in the dissociative bond, and the cc-pVDZ basis for all other atoms in the molecule. The active space, illustrated in figure ESI.5a, comprises of

(1) a σ orbital on the N-H bond

(2) a lone pair on the N atom

(3)–(5) ring π orbitals

(6) σ^* orbital on the N-H bond and

(7),(8) the ring π^* orbitals.

The second potential energy cut, shown in panel B, uses the same (10,8) active space as enumerated above, however it also uses the full aug-cc-pVDZ basis set for all atoms in the molecule, not just the dissociative N and H atoms. The addition of the extra diffuse functions on the other atoms has very little noticeable effect on the potential energy curves, thus confirming the

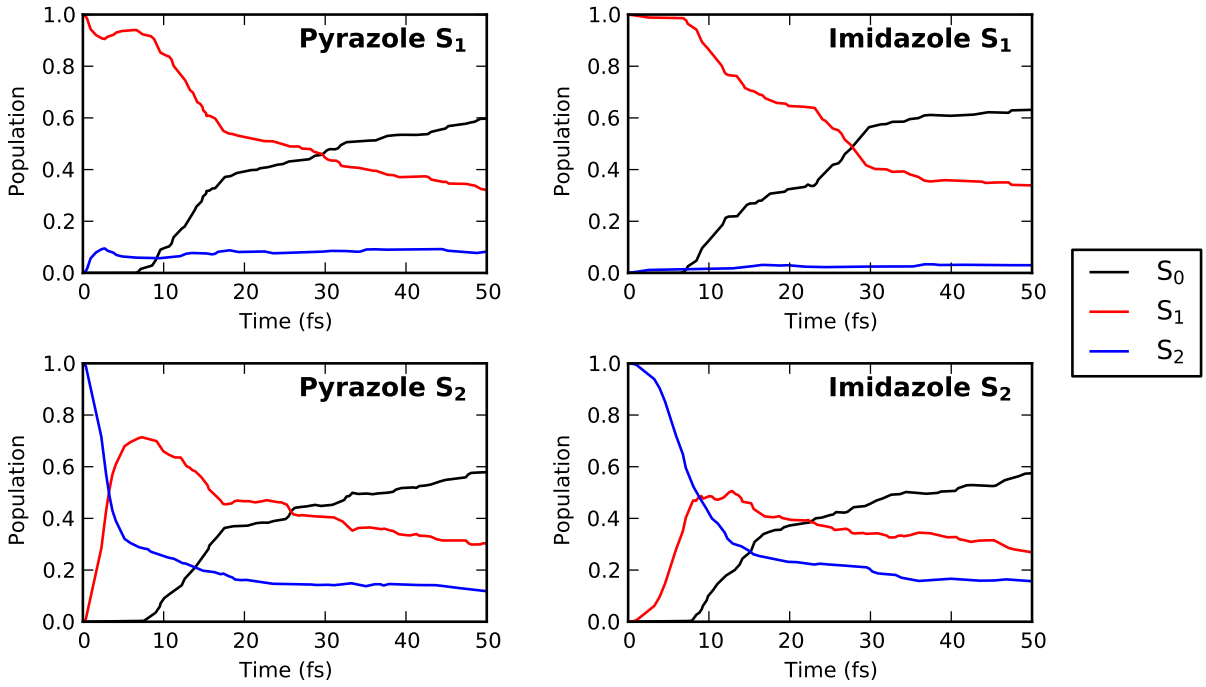

(a) Pyrazole and Imidazole

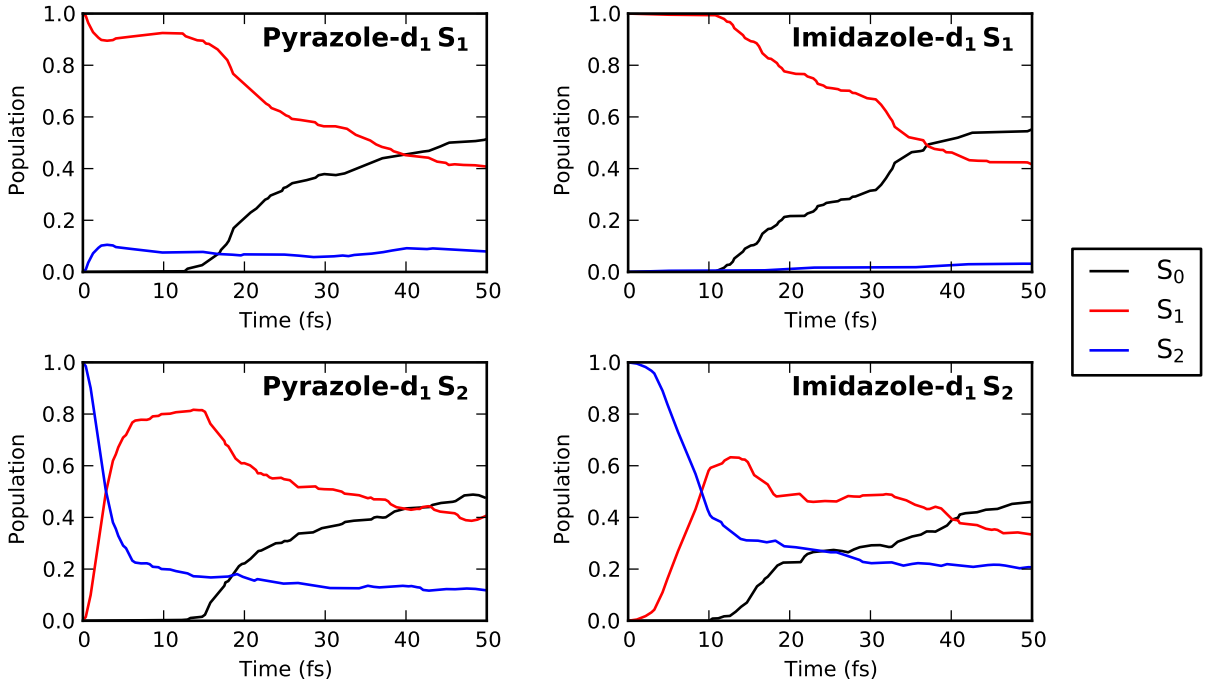

(b) Pyrazole-d_1 and Imidazole-d_1

Figure ESI.1: Comparisons of the electronic populations for the first 50 fs of dynamics from 100 trajectories starting on either the S_1 or S_2 states, tracking population in the S_0 (black), S_1 (red) and S_2 (blue) electronic states.

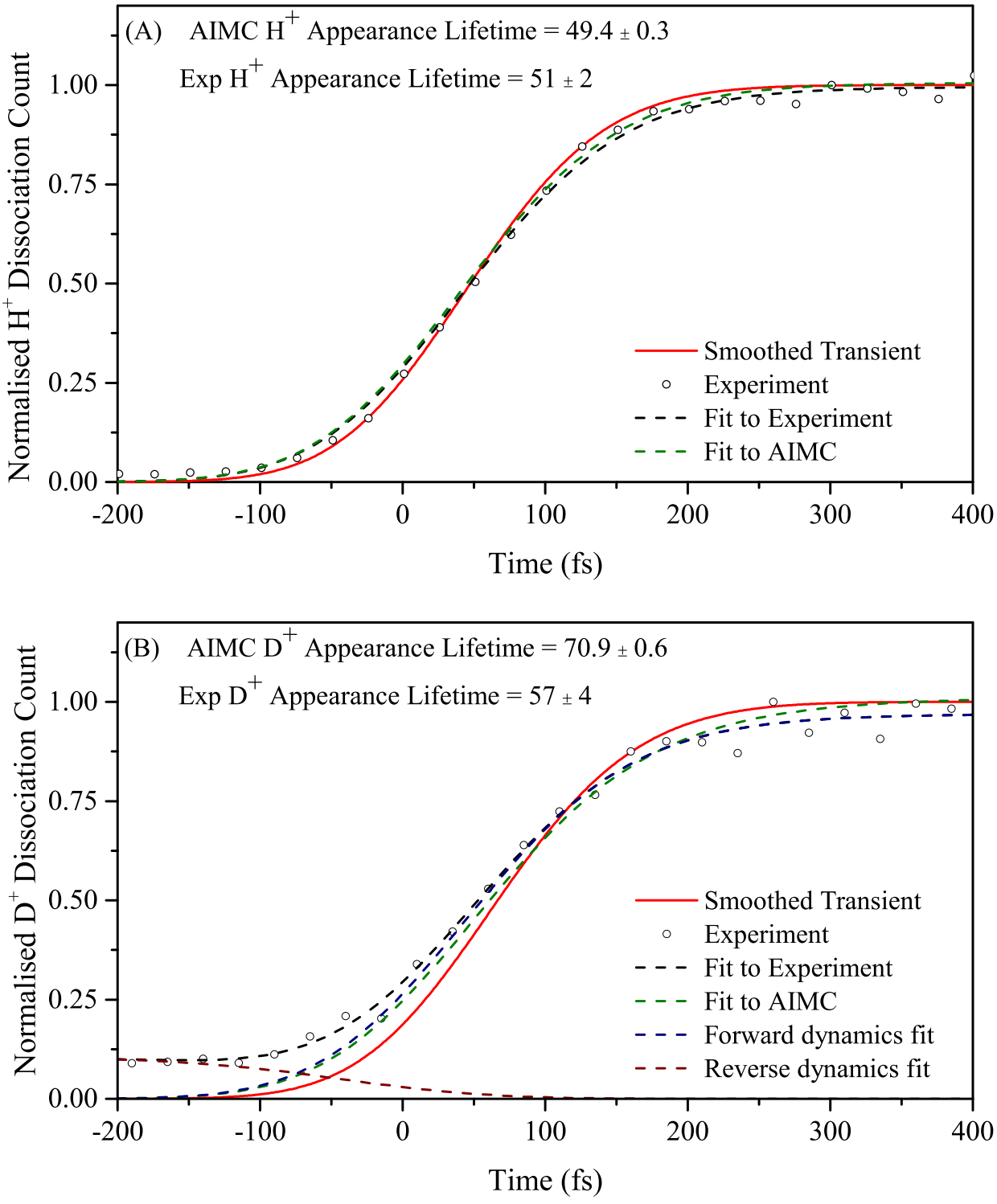

Figure ESI.2: Experimental and AIMC transients for imidazole (A) and imidazole-d_1 (B), shown with the fits to the kinetic model used to find to H/D appearance lifetimes. Also shown on (B) are the decomposed fits showing both the forward and reverse dynamic components to the model.

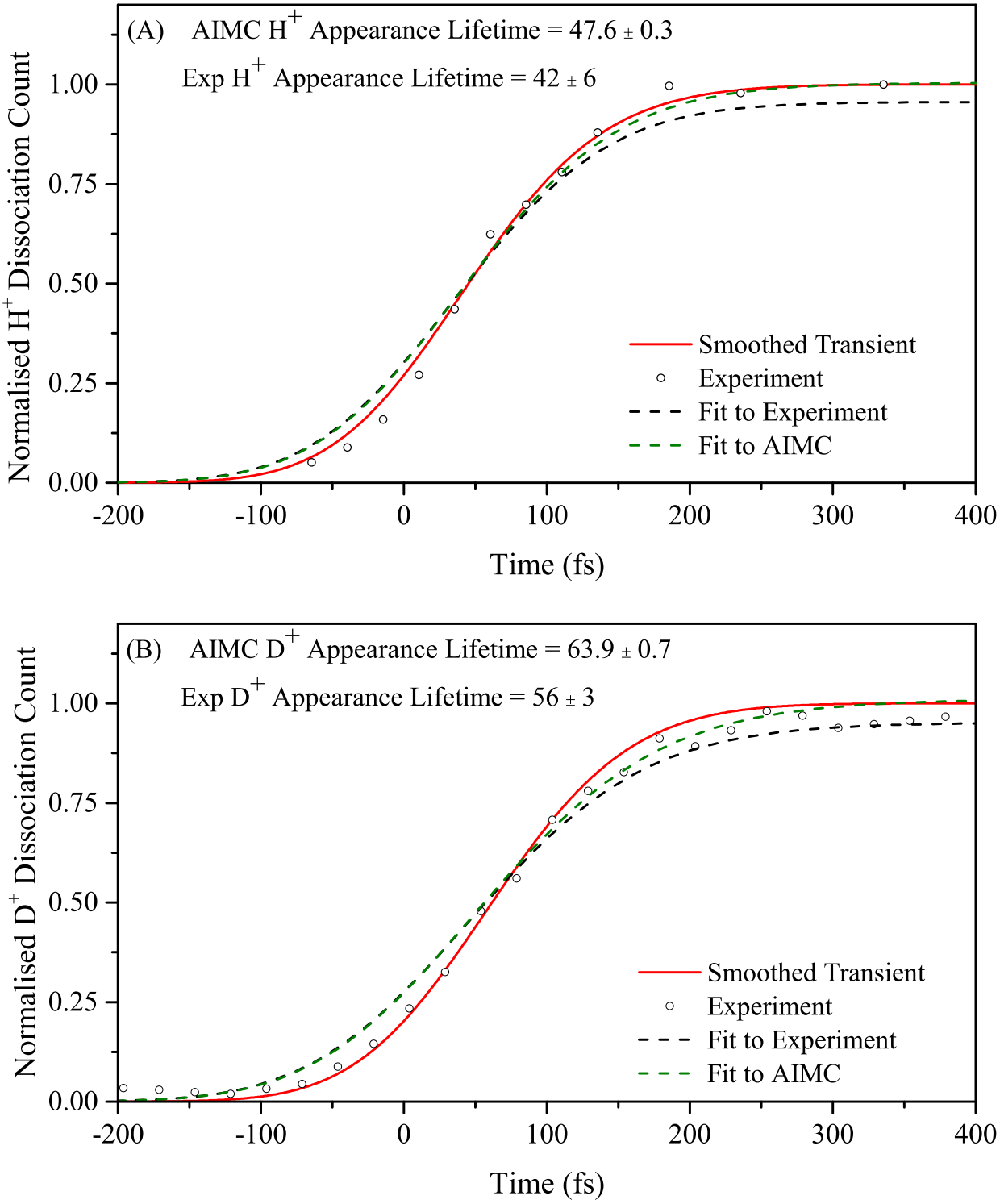

Figure ESI.3: Experimental and AIMC transients for pyrazole (A) and pyrazole-d_1 (B), shown with the fits to the kinetic model used to find to H/D appearance lifetimes.

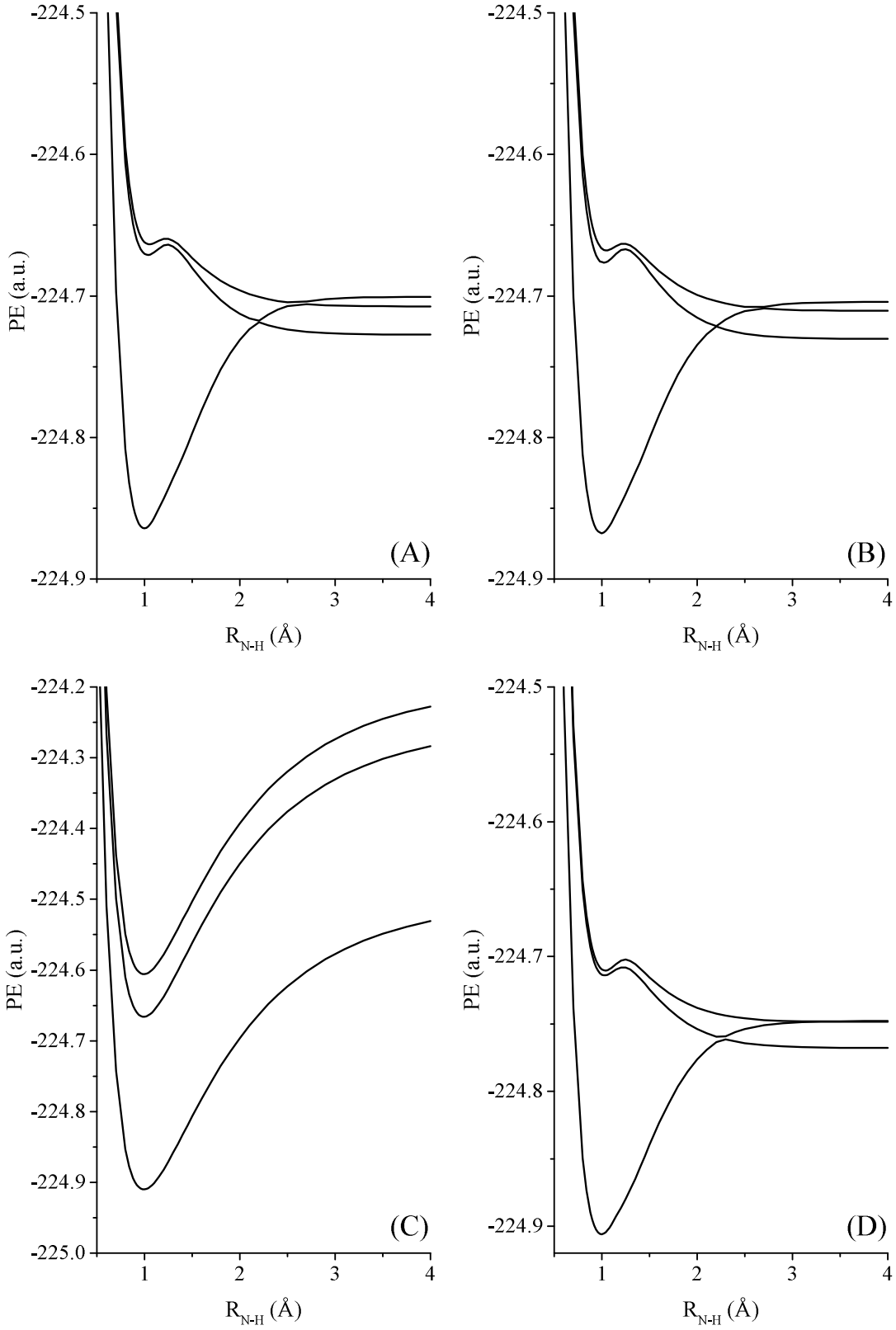

Figure ESI.4: Potential energy cuts along the N-H stretch for pyrazole with different active spaces and basis sets : (A) - (10,8) active space with a mixed aug-cc-pVDZ and cc-pVDZ basis set; (B) - (10,8) active space with full aug-cc-pVDZ basis set; (C) - (10,8) active space with aug-cc-pVDZ basis set in the configuration used in ref 14, i.e. with σ and σ^* orbitals only on the N-N bond; (D) - (12,10) active space with aug-cc-pVDZ basis set with σ and σ^* orbitals on both the N-H and N-N bonds

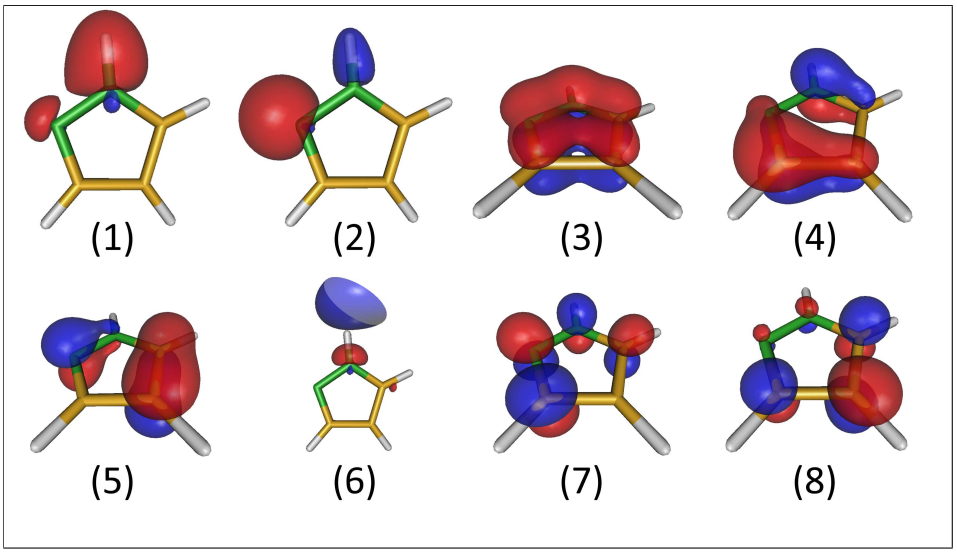

(a) Active space used for the simulation of pyrazole in the main text, and in figure ESI.4 panels (A) and (B)

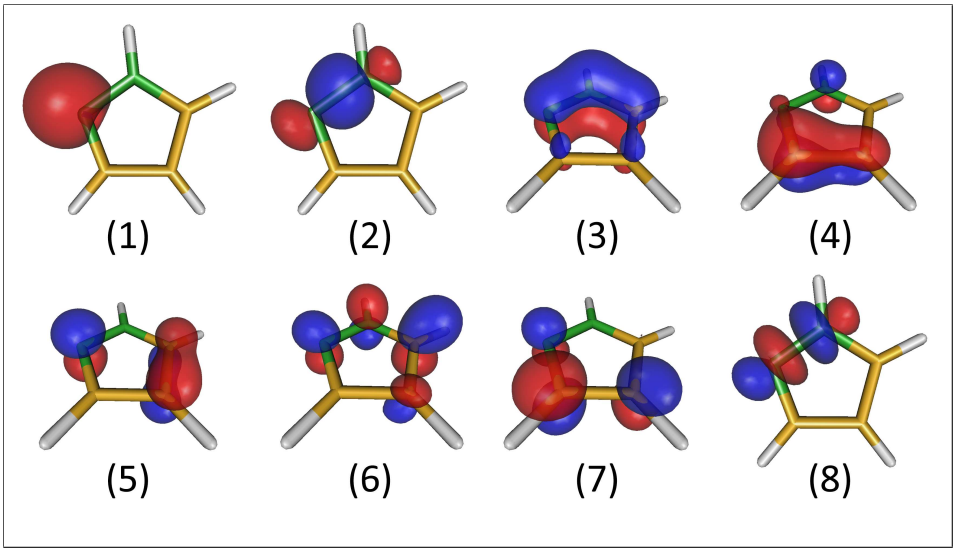

(b) Active space used for the simulation of pyrazole in figure ESI.4 panel (C)

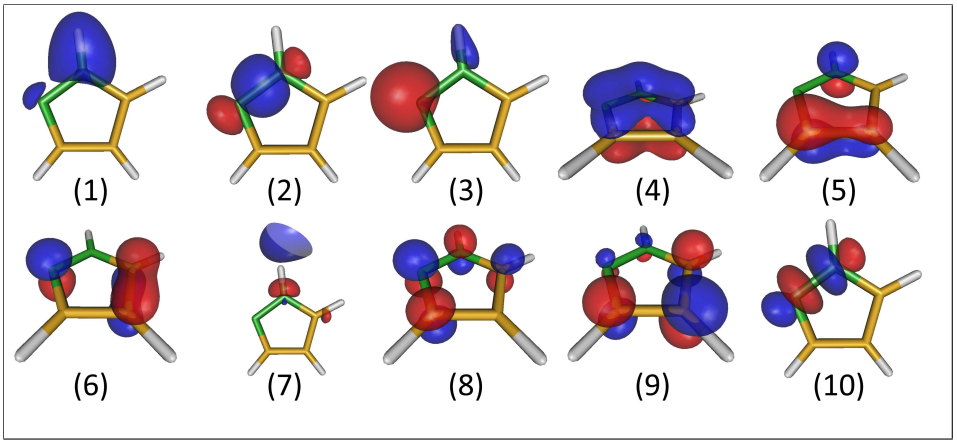

(c) Active space used for the simulation of pyrazole in figure ESI.4 panel (D)

Figure ESI.5: Active spaces used to generate the potential energy cuts along the N-H stretch shown in figure ESI.4

validity of using the aug-cc-pVDZ only on the dissociative N and H atoms when considering N-H photodissociation. Panel C gives the potential energy cuts along the N-H stretch when using a (10,8)/aug-cc-pVDZ active space in the configuration described in the article by Xie *et al.*[14] for their CASPT2 calculations of pyrazole, which is illustrated in figure ESI.5b and comprises of

(1) a lone pair on the N atom

(2) a σ orbital on the N-N bond

(3)–(5) ring π orbitals

(6),(7) ring π^* orbitals

(8) a σ^* orbital on the N-N bond.

It can be clearly seen that when calculated using CASSCF, the intersections between any of the states are removed for this active space along the N-H stretch and the barrier height is greatly increased on all states shown. As such, a simulation using this active space with CASSCF would be incapable of describing any dissociation of the N-H bond. This is in stark contrast to the results given by Xie *et al.* who observe an almost barrierless transition between the $\pi\pi^*$ and $\pi\sigma^*$ states in their MS-CASPT2 calculations, and so could be indicative of differences caused by the level of electronic structure theory used. The final panel, D, shows the potential energy cuts along the N-H stretch for a (12,10)/aug-cc-pVDZ active space which includes σ and σ^* orbitals on both the N-H and N-N bonds. This active space is illustrated in figure ESI.5c and comprises of

(1) a σ orbital on the N-H bond

(2) a σ orbital on the N-N bond

(3) a lone pair on the N atom

(4)-(6) ring π orbitals

(7) a σ^* orbital on the N-H bond

(8),(9) ring π^* orbitals

(10) a σ^* orbital on the N-N bond.

The similarity between panel D and panels A and B is striking, although it can be seen that the energy of the S_1 and S_2 states are lowered slightly. The similarity of these potential energy curves indicates that the larger active space would allow for N-H dissociation in pyrazole just as with the smaller active space shown in panels A and B. This does not, however, give any information about the dynamics on these states and it should be noted that Xie *et al.* saw a barrierless transition between the $\pi\pi^*$ and $\pi\sigma^*$ states along the N-H stretch which was not encountered in their dynamics.

References

[1] D. V. Makhov, W. J. Glover, T. J. Martínez and D. V. Shalashilin, *J. Chem. Phys.*, 2014, **141**, 054110.

[2] D. V. Makhov, K. Saita, T. J. Martínez and D. V. Shalashilin, *Phys. Chem. Chem. Phys.*, 2015, **17**, 3316–3325.

[3] D. V. Shalashilin, *J. Chem. Phys.*, 2010, **132**, 244111.

[4] D. V. Shalashilin, *Faraday Discuss.*, 2011, **153**, 105–116.

[5] A. L. Thompson, C. Punwong and T. J. Martínez, *Chem. Phys.*, 2010, **370**, 70–77.

[6] M. Ben-Nun, J. Quenneville and T. J. Martínez, *J. Phys. Chem. A*, 2000, **104**, 5161–5175.

[7] M. Ben-Nun and T. J. Martínez, *Adv. Chem. Phys.*, 2002, **121**, 439–512.

[8] T. J. Martínez, M. Ben-Nun and R. D. Levine, *J. Phys. Chem.*, 1996, **100**, 7884–7895.

[9] D. V. Makhov, C. Symonds, S. Fernandez-Alberti and D. V. Shalashilin, *Chem. Phys.*, 2017, **493**, 200–218.

[10] D. V. Makhov, T. J. Martínez and D. V. Shalashilin, *Faraday Discuss.*, 2016, **194**, 81–94.

[11] J. A. Green, D. V. Makhov, N. C. Cole-Filipiak, C. C. Symonds, V. G. Stavros and D. V. Shalashilin, (In Press at Phys. Chem. Chem. Phys).

[12] C. Symonds, J. A. Kattirtzi and D. V. Shalashilin, *The Journal of Chemical Physics*, 2018, **148**, 184113.

[13] D. V. Makhov and D. V. Shalashilin, *Chemical Physics*, 2018, **515**, 46–51.

[14] B.-B. Xie, X.-Y. Liu, Q. Fang, W.-H. Fang and G. Cui, *J. Phys. Chem. Lett.*, 2017, **8**, 1019–1024.